PCCP

Gas Adsorption and Light Interaction Mechanism in Phosphorene-Based Field-Effect Transistors

Journal:	*Physical Chemistry Chemical Physics*
Manuscript ID	CP-ART-12-2019-006547.R2
Article Type:	Paper
Date Submitted by the Author:	21-Feb-2020
Complete List of Authors:	Rajapakse, Manthila; University of Louisville, Department of Physics and Astronomy Anderson, George; University of Louisville, Department of Physics and Astronomy Zhang, Congyan; University of Louisville, Physics and Astronomy Musa, Rajib; University of Louisville, Department of Physics and Astronomy Walter, Jackson; Universiyty of Louisville, Conn Center for Renewable Energy Research Yu, Ming; University of Louisville, Department of Physics and Astronomy Sumanasekera, Gamini; University of Louisville, Physics Jasinski, Jacek; Universiyty of Louisville, Conn Center for Renewable Energy Research

SCHOLARONE™
Manuscripts

Physical Chemistry Chemical Physics

ARTICLE

Gas Adsorption and Light Interaction Mechanism in Phosphorene-Based Field-Effect Transistors

Received 00th January 20xx,
Accepted 00th January 20xx

DOI: 10.1039/x0xx00000x

www.rsc.org/

Manthila Rajapaksa,[a] George Anderson,[a] Congyan Zhang,[a] Rajib Musa,[a] Jackson Walter,[b] Ming Yu,[a] Gamini Sumanasekera[a,b] and Jacek B. Jasinski *[b]

Phosphorene-based field effect transistor (FET) structures were fabricated to study the gas- and photo-detection properties of phosphorene. The interplay between device performance and environmental conditions was probed and analyzed using *in-situ* transport measurements. The device structures were exposed to different chemical and light environments to understand how they perform under different external stimuli. For the gas/molecule detection studies, inert (Ar), as well as, oxidizing (N_2O), and reducing (H_2 and also N_2H_4) agents were selected. The FET structure was exposed to these different gases, and the effect of each gas on the device resistance was measured. The study showed varying response towards different molecules. Specifically, no significant resistance change was observed upon exposure to Ar, while H_2 and N_2H_4 were found to decrease the resistance and N_2O had the opposite effect resulting in an increase in resistance. This work is the first demonstration for the detection of N_2H_2 and N_2O using a phosphorene-based system. These phosphorene-based FET structures were also found to be sensitive to light exposure. When such structure was irradiated with light, the current modulation was lost. The observed resistance changes can be explained as a result of the modulation of the Schottky barrier at the phosphorene-electrical contact interface due to the adsorbed molecules and charge transfer, and/or photo-induced carrier generation. The results were consistent with the transfer characteristics of V_{ds} vs V_g.

Introduction

Gas sensors have many applications in public safety, environmental monitoring, and air quality control.[2-6] Especially important are gas sensors that operate at room temperature. The majority of gas sensors are based on the principle that the gas species absorbed onto the material cause a change in the sensor resistance. A good sensor will have high sensitivity, short response and recovery time, low detection limit, high selectivity, and good stability. There are two common types of gas sensors known as field effect transistor (FET) and chemiresistor. Two-dimensional (2D) materials have emerged as promising candidates for this application due to their large surface-to-volume ratios and high surface activities.[7-10] Since the discovery of graphene, many 2D materials such as graphene oxide, sulfides (MoS_2 and WS_2) and selenides (WSe_2 and $MoSe_2$) have been used to fabricate gas-sensing devices.[11, 12] Theoretical studies based on density function theory (DFT) have also been carried out in different aspects of gas adsorption such as gas capturing strength of different 2D materials and reversibility of adsorption.[13] Black phosphorus (BP), particularly in its 2D form, i.e., phosphorene, has been shown to be sensitive to the surrounding atmosphere and can be used to detect different gas molecules.[14-17] Kou et al.[17] first predicted that BP would be a better gas sensor than other 2D materials and would be more sensitive to nitrogen-based molecules. Later, Abbas et al.[14] have fabricated the first BP gas sensor configured as an FET-based sensor. Their BP sensor have shown high sensitivity to NO_2 in an argon atmosphere and a response time comparable to a MoS_2. Studies by Cui et al.[16] have shown that the sensitivity of the BP FET sensor depended on the thickness of the nanosheet and that the sensor performed best when the thickness was 4.8 nm. They have also shown a high selectivity to NO_2 in the presence of H_2, CO, and H_2S gases. Donarelli et al.[18] have fabricated a chemiresistor gas sensor and have demonstrated good sensitivity to NO_2, NH_3, and H_2, but no response to CO or CO_2. Feng et al.[19] has increased the sensitivity of BP 5-6 times by constructing a hetero-structure gas sensor based on few-layer phosphorene and MoSe2 flakes on the same chip. Shi et al.[20] have improved the stability and versatility of sensing of a phosphorene-based FET gas sensor by using few layer BP, boron nitride and MoS_2 as the top-gate, dielectric layer and conduction channel, respectively. Theoretical studies have shown that alkali-atom (Na and Li) doped phosphorene can have significantly enhanced gas sensitivities over pristine phosphorene.[21] The structure of BP makes this material extremely flexible. Kistanov et al. have shown that rippled phosphorene (formed by applying a compressive strain) exhibits enhanced physisorption of NO molecules at the top and bottom ripple peaks, thus suggesting strain-tunability of phosphorene gas sensing.[22]

a. Department of Physics and Astronomy, University of Louisville, Louisville, KY, 40292, USA.
b. Conn Center for Renewable Energy Research, University of Louisville, Louisville, KY, 40292, USA. E-mail: jacek.jasinski@louisville.edu; Tel: +1-502 852 6338.
Electronic Supplementary Information (ESI) available: [details of any supplementary information available should be included here]. See DOI: 10.1039/x0xx00000x

Black phosphorous, particularly its 2D form, has also demonstrated the capability for efficient photodetection. Photodetectors convert light into electrical signals, and are used in a variety of ways, such as optical communications, imaging, optical guidance, remote sensing, and more. Various 2D materials have been tested for this application, although it is difficult to obtain high responsivity and ultrafast response covering broad ranges of detection in the electromagnetic spectrum. BP has shown to be a possible option to increase the detection range with significant responsivity due to the tunable direct bandgaps between graphene and transition metal dichalcogenides (TMDs). The first study on BP photodetectors based on FETs have been conducted by Buscema et al.[23] who have discovered that the responsivity and f3dB decreased with increasing excitation and that BP had a sizeable response to ultraviolet (UV), mid-infrared (MIR), and terahertz (THz) spectral regimes. Another study by Wu et al.[24] has shown that ultrathin BP could be an excellent UV photodetector with a significantly enhanced responsivity, exhibiting however a long response time close to 200 s. Guo et al.[25] have developed a MIR photodetector based on BP nanosheets 10 nm thick and demonstrated that a BP photodetector can operate in a broad wavelength range with high responsivity. The main problem with the application of few-layer BP sensors is that BP is unstable in air and undergoes degradation. However, a study by Na et al.[26] has shown that a BP photodetector could be protected against air exposure and degradation byAl_2O_3 passivation.

Here, we report study of chemical and light sensing properties of FET structure with phosphorene as the conducting channel, p-doped Si as the gate, and SiO_2 as the insulating barrier between the channel and the gate. For the chemical sensing, we have selected agents with different reducing/oxidizing properties, including Ar (inert gas), H_2 and N_2H_4 (reducing agents), and N_2O (oxidizing agent). The results on argon and hydrogen adsorption are consistent with previous works. However, there are no experimental nor theoretical work on adsorption of N_2H_4 or N_2O on phosphorene. Our group has published several papers on adsorption of N_2H_4 on single wall carbon nanotubes[27], WS_2[28] as well as N_2O adsorption on WO_3 nanowires[29], carbide derived carbon sensors[30] and graphene[31]. Therefore, based on our expertise from prior research and to shed new insight, we have included the experimental and theoretical investigation of adsorption of N_2O and N_2H_4 on phosphorene. As detailed in this report, our study show a varying response towards different molecules, and for the first time the use of such a phosphorene-based system is demonstrated for the detection of N_2H_2 and N_2O. The sensing mechanism is explained as a result of the modulation of the Schottky barrier at the phosphorene-metal interface.

Results and discussion

Typical characterization results obtained from our exfoliated black phosphorous samples are summarized in Fig. 1. The samples consisted of few-micrometer-large flakes, like the one shown in the high angle annular dark filed (HAADF) image in Fig. 1a. The energy-dispersive x-ray spectroscopy (EDS) confirmed that the flakes were composed of pure phosphorous, as shown in Fig. 1b,c, where the elemental mapping and the EDS spectrum of the flake from Fig. 1a are presented, respectively. The crystal structure was confirmed by high-resolution transmission electron microscopy (HRTEM) and selected area electron diffraction (SAED). A TEM image of the flake from Fig. 1c is shown in Fig. 1d. The HRTEM analysis (Fig. 1e,f) revealed two sets of perpendicular lattice fringes, one with the *d*-spacing of ~3.3 Å and the other of ~4.4 Å. These values match (within the experimental errors) the *d*-spacing values of 3.314 and 4.373 Å for the (100) and (001) planes of the orthorhombic black phosphorous (ICDD PDF # 00-047-1626), respectively. The analysis indicates also that the flake's normal is perpendicular to the [010] direction, i.e. to the *b*-axis of black phosphorous structure. This is in agreement with the [010] zone axis indexing of the SAED pattern in inset of Fig. 1d. The observed exfoliation along the *xz* planes, i.e., in the direction perpendicular to the *b*-axis, is consistent with the structure of black phosphorous, consisting of layers stacked and weakly bonded along the *b*-axis. This is also confirmed by the comparison between the x-ray diffraction (XRD) pattern from bulk material (Fig. 1g) and the SAED ring pattern of one of the exfoliated samples (Fig. 1h and its inset). While the XRD pattern of the bulk sample shows all BP (ICDD PDF # 00-047-1626) peaks, the SAED pattern of the exfoliated material exhibits the systematic absence of the (0*k*0) reflections, which indicates that the flakes have the [010] normal.

The exfoliated BP was used to fabricate a phosphorene-based FET device structure, as the one shown schematically in Fig. 2a, and was then studied for its gas- and photo-sensing performance. The Aluminium contacts of the interdigitated contact pattern serve as the source and the drain of the FET device while the p-doped Si serves as the back gate. Electrical measurements were carried out using a Keithley 6487 picoammeter/voltage source which has the current resolution of 10 fA. The room temperature I-V characteristics and the plot of relative changes in resistance

$$\frac{\Delta R}{R} = \frac{R(T) - R_{RT}}{R_{RT}} \qquad (1)$$

vs. temperature, T, where R_{RT} is the room temperature resistance, are shown in Fig. 2b,c. The resistance was measured between the source and the drain at zero gate voltage (V_g=0). The non-linear behaviour of the I-V curve (Fig. 2b) indicates the formation of a Schottky barrier at the phosphorene-aluminium contact interface. A decrease in resistance vs. temperatures shown in Fig. 2c is typical for semiconductors as more charge carriers are thermally excited across the energy band gap at elevated temperatures. The vacuum transport measurements were followed by the in-situ electrical studies upon exposure of the FEG structure to various gas and light conditions. During gas exposure, the conducting channel of the FET (phosphorene) was held at "ON" by setting V_g = -20 V and drain-source voltage, V_{ds} = 0.2 V for resistance measurements.

This journal is © The Royal Society of Chemistry 20xx

Please do not adjust margins

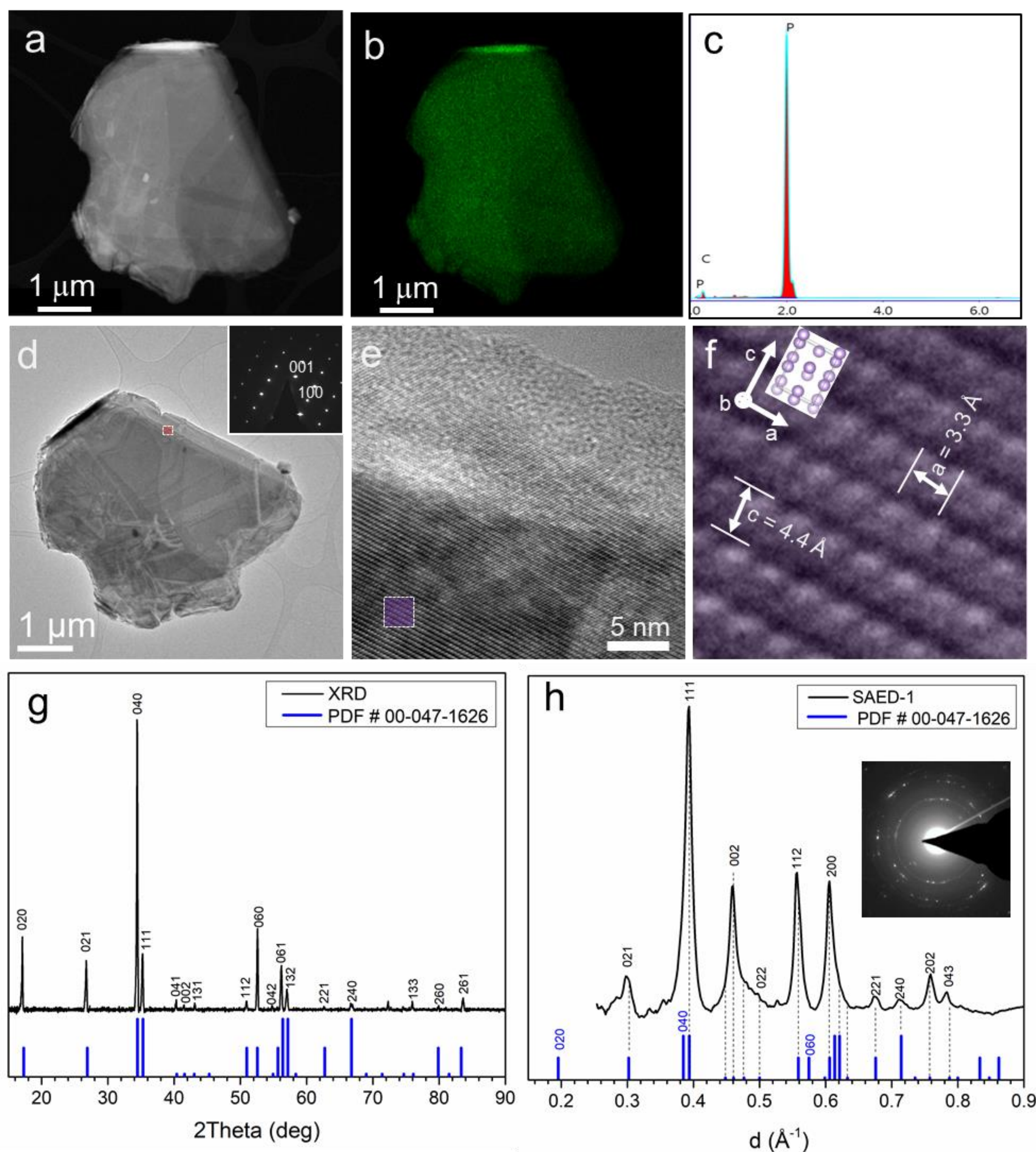

Fig. 1 (a) HAADF image of a single BP flake. (b) Phosphorous elemental and (c) EDS spectrum of the flake shown in (a). (d) TEM image of the flake shown in (a). SAED of the flake is shown in the inset. (e) HRTEM image of the red boxed are shown in (d). (f) Zoomed-in image of the violet boxed region shown in (e). Crystallographic directions and the atomic model of the unit cell are shown schematically in the upper-left region. (g) XRD pattern of bulk black phosphorous. (h) Rotational average curves extracted from SAED ring patterns of exfoliated flakes. A typical SAED ring pattern is shown in the inset.

Fig. 3a shows the relative change of resistance when exposed to Ar, N_2O, H_2, and N_2H_4 at room temperature. As expected, Ar did not show any measurable change in the resistance. When N_2O was admitted to a pressure of 12 Torr, the resistance increased by ~25 % from its initial value. Upon pumping, the resistance recovers to the original value. Next, when N_2H_4 was admitted to a pressure of 12 Torr, the resistance dropped by ~40 % and again recovered its original value upon pumping. Finally, when exposed to H_2 to the same pressure (12 Torr), the resistance decreased by ~ 70% and recovered upon pumping. As shown in Figure 3a, the adsorption and desorption can be fitted with double-exponential functions, indicating existence of two time

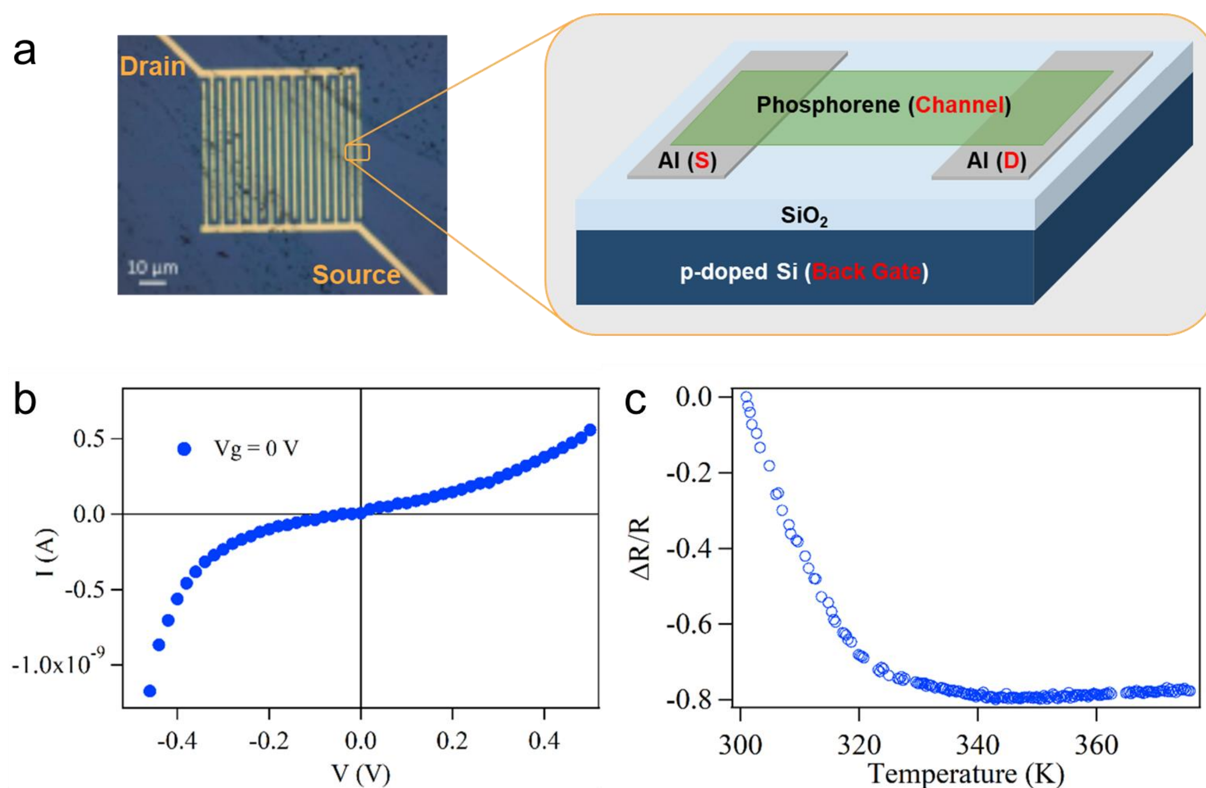

Fig. 2 (a) Optical microscopy image (left) and schematic (right) of a phosphorene FET structure Two Aluminium contacts serve as the source and the drain while the p-doped Si serve as the back gate. (b) *I-V* curve at V_g=0 at room temperature (c) Relative changes in the resistance of phosphorene versus temperature.

constants corresponding to two different adsorption sites with varying binding energies.

FET transfer curves of the device were also measured under vacuum and various gas environments. We supplied a fixed bias of 0.2 V between the source and the drain and swept the gate voltage from –20 to 5 V. The results demonstrate that the device state switched from 'on' to 'off' state with a current drop up to several orders. The two-terminal transfer curves (I_{ds}–V_g, where I_{ds} is drain-source current and V_g is gate bias) of phosphorene in different gases (at a fixed V_{ds} = 0.2 V) are shown for the back gate voltage, V_g ranging from -20 V to 5V in Fig. 3b. Next, the maximum resistance change for each gas (from Fig. 3a) was plotted against the shift of the gate voltage (estimated at I_{ds} = 3 x 10^{-9} A in Fig. 3b) with respect to the vacuum value for each gas as shown in Fig. 3c. The transfer curves in Fig. 3b show large currents at negative gate values and decrease by several orders of magnitude at small positive gate voltages. However, no saturation nor subsequent increase in I_{ds} in the measured positive voltage range is observed and believed to be due to the Schottky barrier at the interface between the electrode and phosphorene of the FET device which suppresses the charge transport.[16] The measured transfer characteristics showing the decrease of the current values when the gate voltage became increasingly positive is characteristic of the typical behaviour of a p-type FET due to the depletion of the majority holes in a p-type material at positive gate voltages.[16] For the pristine sample, it is shown that flat-band condition occurs at about V_g = -16.5 V. This rapid modulation of current is in contrast to previous works that reach flat band condition at much higher gate voltage values.[23, 32, 33] Transfer characteristics after Ar exposure show a slight increase in the flat band voltages compared to the pristine phosphorene. The exposure to N_2O, N_2H_4, and H_2 result in progressively increasing flat band voltages consistent with resistance changes.

Changes in the electrical transport properties of phosphorene show the most pronounced effects when exposed to H_2. The hydrogen/phosphorene interaction has been calculated to be a physisorbed process that is reversible.[34, 35] Hydrogen is a highly reducing gas, i.e., it is expected to donate electrons and for a p-type semiconductor this should result in increased resistance and a decrease in current, as holes are depleted. That is true for a charge transfer process during physical absorption. N_2O on the other hand is a strong electron acceptor and should lead to the decrease of the resistance. However, Fig. 3a shows the opposite behaviour.

In order to understand the gas-phosphorene interaction, we carried out DFT calculations. A 3×3 supercell was chosen to study the adsorption of foreign gases (H_2, N_2H_4, and N_2O, respectively) on phosphorene monolayer. The gas molecules are initially placed on the top of P atoms with shortest distance of ~ 1.5-1.9 Å, but during relaxation the molecule moves away from the phosphorene and stabilized at the shortest distance of

This journal is © The Royal Society of Chemistry 20xx

Please do not adjust margins

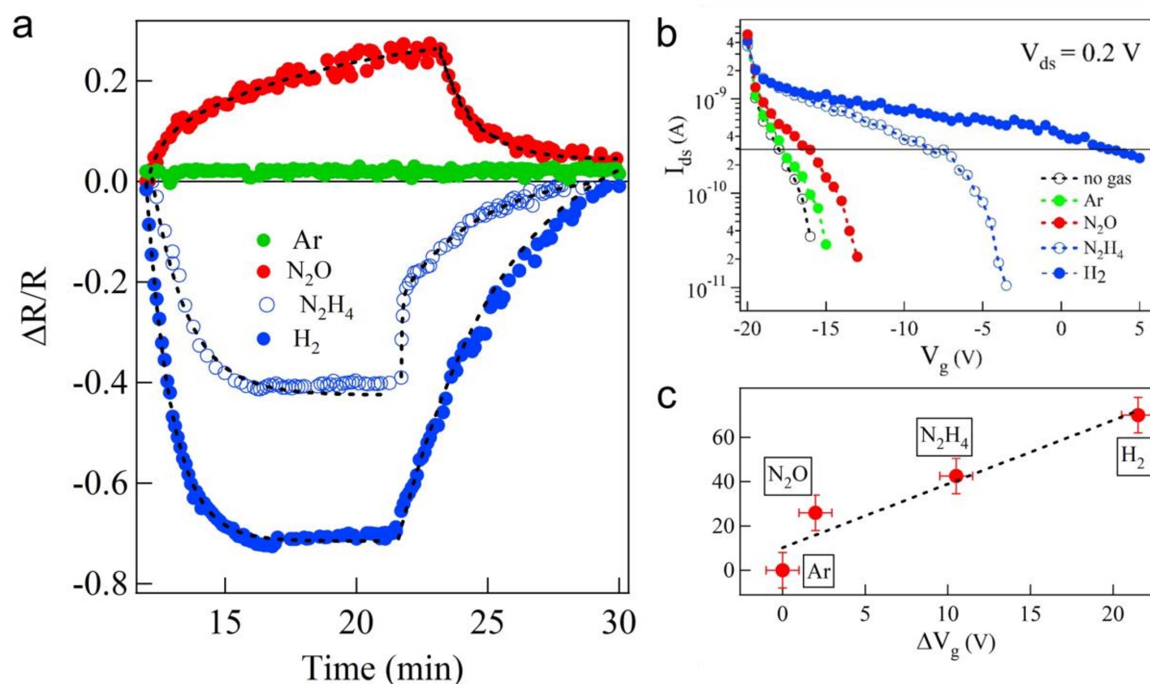

Fig. 3 (a) Relative change in resistance and (b) transfer characteristics as phosphorene is exposed to various gases (Ar, N_2O, H_2) and N_2H_4 at room temperature. (c) The plot of the resistance change vs gate voltage difference relative to the value for Ar, all measured at $I_{ds} = 3 \times 10^{-9}$ A.

~2.77-3.6 Å (Fig. 4a), clearly showing a physical adsorption nature. The corresponding adsorption energy (E_a) per gas molecule, calculated for such systems are -0.246, -0.432, and -0.354 eV for H_2, N_2H_4, and N_2O, respectively. These values are in the range typical for physical adsorption. The charge redistribution in the real space and the interaction between adsorbates and phosphorene are analysed in terms of the differential charge densities (DCD) of the combined systems (Fig. 4b). Both the gas molecules and phosphorene are polarized and a small amount of charge transfer from phosphorene to the gas molecule (i.e., 0.019e for H_2, 0.045e for N_2H_4, and 0.052e for N_2O, respectively) is found. The calculated electronic band structures for phosphorene exposed to various gas molecules (Fig. S1 (left)) show no impurity state associated with the gas molecules pining into the band gap, but instead, such states are in the deep valence band, which can be clearly seen from the partial densities of states (PDOS) in Fig. S2 (right). These results indicate that the electronic band structure of phosphorene near the Fermi level will not be affected significantly even when it is exposed to the foreign gas molecules.

We explain the observed behaviour as due to the modulation of the Schottky barrier formed at the phosphorene-aluminium contact interfaces as described below. Band bending phenomenon associated with bringing a metal and a semiconductor in contact lead to the Schottky barrier formation. As shown in Fig. 5, the conduction band and the valance band are bent upward due to the electron transfer from aluminium electrodes to p-type phosphorene. There is a barrier against the hole flow from the semiconductor to the metal.

Phosphorene drop cast from dispersion (in dimethylformalhide (DMF)) on top of the contacts likely forms a Schottky barrier. The work functions of phosphorene and aluminium differ. When phosphorene is in contact with metals, electrons will transfer from one (higher energy) to the other (lower energy) to equilibrate the Fermi levels. The Schottky barrier height is determined (in the simplest terms) by

$$\phi_{SB} = \phi_M - \mathrm{X} \qquad (2)$$

, where ϕ_M is the work function of aluminium and X is the electron affinity of phosphorene. Fig. 5 shows the schematic diagram of the Schottky barriers for varying number of phosphorene layers (1, 3, and 5) with aluminium.[1] As expected, the Schottky barrier height (ϕ_{SB}) decreases as the number of layers increases from its value of ~1.23 eV for monolayer phosphorene.

The change in the Schottky barrier height can be understood by the change of the metal (aluminium) work function as well as the semiconductor (phosphorene) work function as a result of gas molecule absorption (Fig. 6). Previous studies have shown that the work function of Al can be decreased by N_2H_4 and increased by N_2O. Therefore, in the monolayer phosphorene device, the Schottky barrier height at the Al/phosphorene junction can be reduced to allow more holes under N_2H_4 and H_2 exposure and the opposite effect can take place under N_2O exposure. This difference confirms the Schottky barrier formation and its modulation under ambient gas condition. Charge transfer between the gas molecules and phosphorene

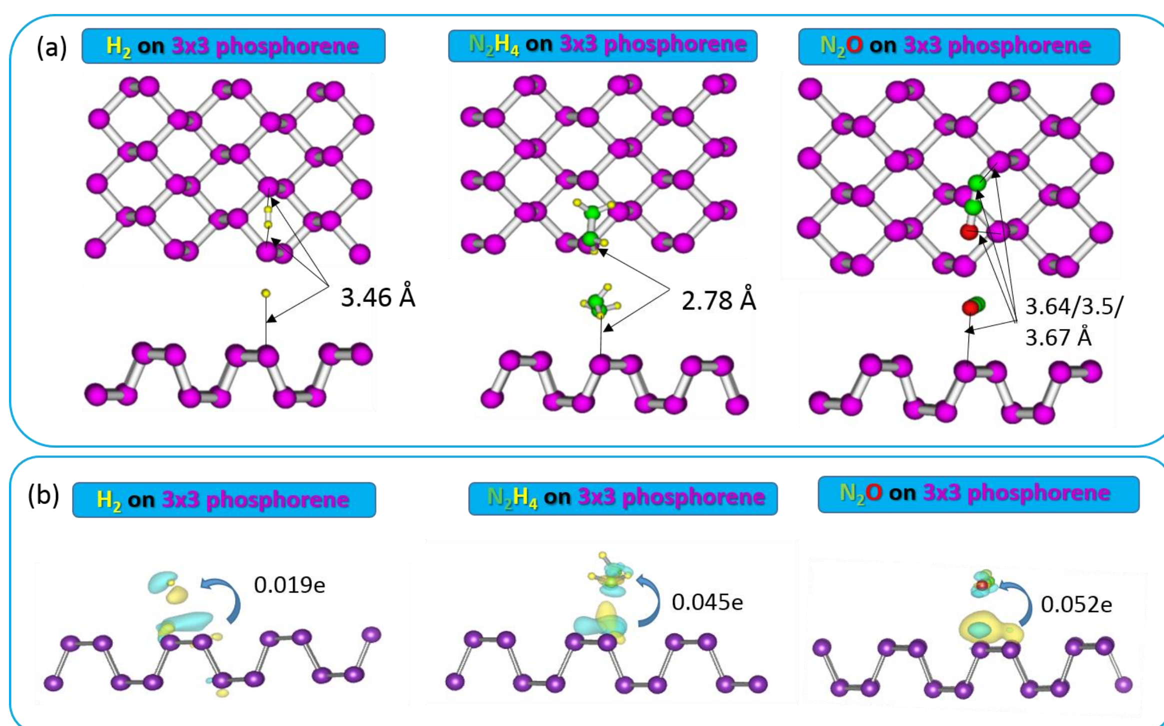

Fig. 4 (a) Optimized atomic models from the DFT calculations of gas molecule adsorption of H_2 (left), N_2H_4 (middle), and N_2O (right) on the surface of 3x3 supercell of phosphorene. (b) Side views of DCD for H_2 (left), N_2H_4 (middle), and N_2O (right) molecules interacting with the surface of phosphorene. The isosurface level for H_2, N_2H_4, and N_2O is taken as 7×10^{-5} e/Å^3, 8×10^{-4} e/Å^3, and 2×10^{-4} e/Å^3, respectively. The electron accumulation (depletion) region on the DCD isosurface is indicated by yellow (blue). The directions (indicated by the arrows) and values of charge transfer are shown.

influence the Schottky barrier height. N_2O is a strong electron acceptor, while N_2H_4 and H_2 are electron donors to phosphorene. N_2O is increasing the Schottky barrier due to withdrawal of electrons and increased p-doping in phosphorene. The increased Schottky barrier causes the hole conduction more difficult, which in turn increases resistance of such device structure (with Al contacts). The resistance of the device on the other hand decreases upon exposure to N_2H_4 and H_2. This is because N_2H_4 and H_2 donate electrons to phosphorene, thus decreasing its Schottky barrier. The measured gas sensitivity of N_2H_4 and H_2 are higher than that of N_2O. Further, exposure to H_2 shows much higher decrease in resistance in comparison to N_2H_4, implying phosphorene/Al interface showed lower ϕ_{SB} values for H_2 compared to N_2H_4.
These phosphorene-based FET structures were also used to study light interaction properties of phosphorene. The structures were illuminated with light emitting diodes (LEDs) with different wavelengths while their electrical characteristics were measured under such conditions. Fig. 7a and Fig. S3 show how the electrons are excited by the LED light. We used the same current value (different voltage values) to power each LED. Red light having photon energy of 1.65 eV to 2.00 eV is comparable to the band gap of phosphorene and the Schottky barrier height while yellow light photon energies of 2.10 eV to 2.17 eV are slightly higher. Both red and yellow light appear to be capable to excite the charge carriers. The measurements also showed the decrease in hole concentration and the loss of current modulation due to light, which is the evidence that the light sources are generating charge carriers in phosphorene. As more charge carriers are excited, current modulation is no longer possible. Also, short lived excited electrons may increase recombination of holes. The response times of 6.5 s (ON) and 8.5 s (OFF) for yellow LED and 6.0 s (ON) and 6.5 s (OFF) for red LED were obtained from fitting with single-exponential functions (Fig. S4). We have also shown the relative changes of resistance of phosphorene exposed to yellow (a) and red (b) LEDs, powered at different bias voltages in Fig. S3.
Fig. 7b shows the schematic diagram of the photocarrier generation in the semiconductor and at the Schottky barrier. Since the incident photon energy is higher than the Schottky barrier height, $\phi_{SB,}$ it can overcome the barrier for the hole and introduce holes into the valence band of phosphorene. At the same time, band-to-band transitions generate equal number of holes and electrons in the valence and conduction band respectively. However, the holes will be trapped in the center of the flat band while electrons in the depletion region drifting to the metal contact and flowing in the external circuit.

Experimental

Fabrication of Phosphorene

Phosphorene samples were obtained using liquid mechanical exfoliation. First, BP crystals were synthesized through a short transport growth method.[36] For this, red phosphorous, SnI_4, and tin, which were used as precursors, were loaded to a quartz tube, which then was evacuated and sealed using oxy flame. The tube was then annealed in a tube furnace in a temperature

This journal is © The Royal Society of Chemistry 20xx

Please do not adjust margins

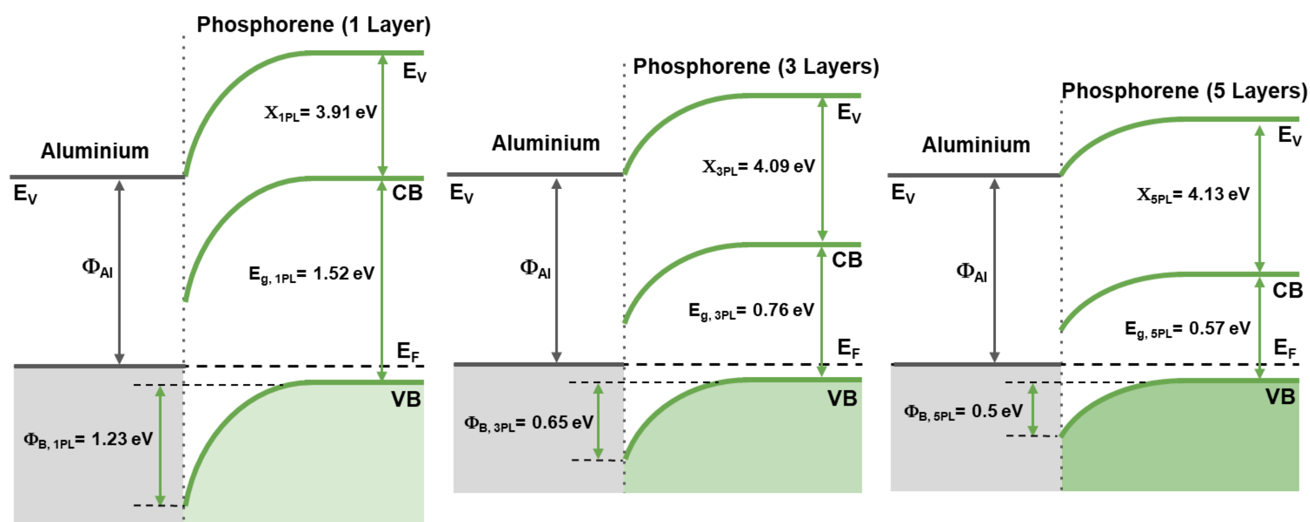

Fig. 5 Schematic of band diagram showing how the Schottky barrier is formed between phosphorene and Al contacts (After Ref.[1]).

gradient, which lead to the formation of black phosphorous crystals. Liquid mechanical exfoliation (LME) was used to fabricate phosphorene flakes. For this, BP powder samples were suspended in DMF and sonicated for 1-4 hours. The suspensions were then centrifuged at 4000-10000 rpm for 30 minutes to produce different fractions of phosphorene flakes. Details of the experimental setups and methods used for the synthesis of black phosphorus and for its LME and centrifuging are described elsewhere.[37]

Characterization

The as-grown and exfoliated BP samples were thoroughly characterized using a wide range of techniques, including XRD, HAADF, HRTEM, EDS, and SAED. For the XRD, the as-grown BP crystals were grinded into a fine powder using agate pestle and mortar. In order to minimize the material degradation, the grinding was done in a glovebox, under a controlled argon atmosphere, and the obtained powder was then placed on a glass slide, covered, and tightly sealed from the top and sides with a scotch tape.

The XRD measurements were performed using a Bruker Discovery D8 system and Cu K_α x-radiation with a wavelength of 1.5406 Å. The HAADF, HRTEM, and SAED measurements were performed using a FEI Tecnai F20 field emission-gun transmission electron microscope under 200 kV of acceleration voltage. This microscope together with the attached EDAX TEAM EDS system was also used for the acquisition of EDS spectra and elemental maps. TEM samples were prepared by drop-casting and drying DMF-based dispersions of exfoliated flakes onto TEM copper grids coated with holey carbon films. For the analysis of SAED ring patterns, rotational average x-y curves were obtained using the DiffTools software.[38]

FEG Fabrication and In-situ Transport Measurements

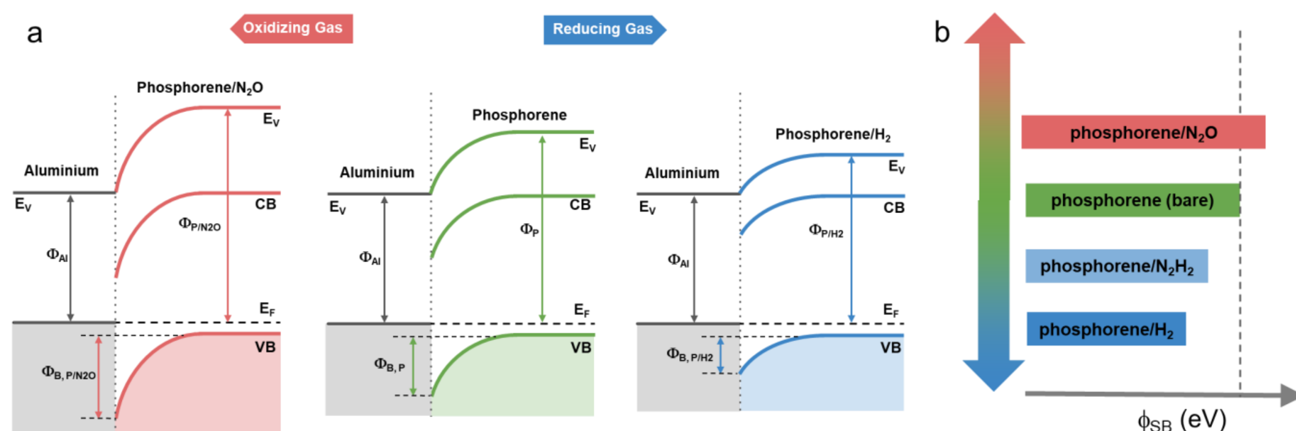

Fig. 6 a) Schematic diagram of the Schottky barrier modulation due to various gasses and chemicals (b) A schematic change of Schottky barrier height due to various gasses according to the resistive changes.

This journal is © The Royal Society of Chemistry 20xx

Please do not adjust margins

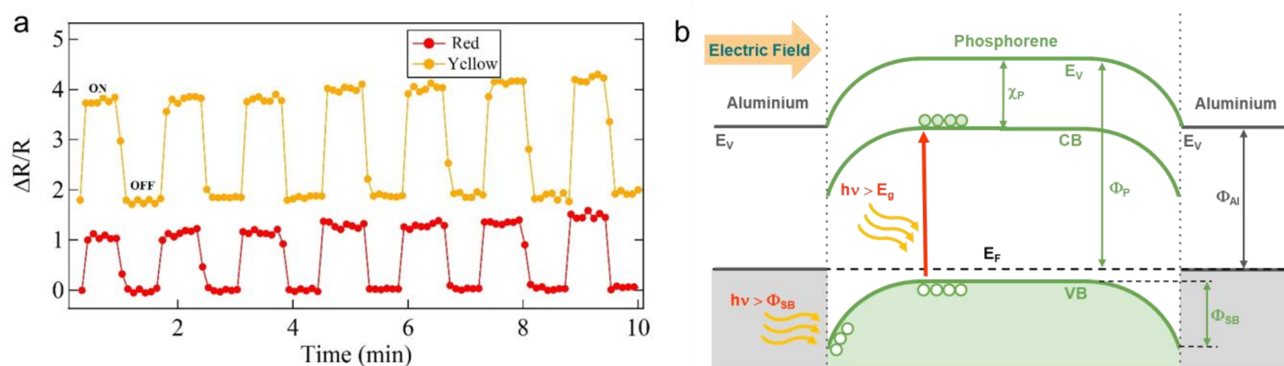

Fig. 7 (a) Relative resistance of phosphorene exposed to red and yellow LEDs. (b) Schematic band diagram depicting the population of the bands with photo generated charge carriers (i) hole population of the valence band overcoming the Schottky barrier (ii) electron-hole pair generation overcoming the band gap.

For the FET fabrication, phosphorene was drop-cast from DMF dispersion onto an interdigitated Al contacts that had previously been deposited on SiO_2/Si substrates. The SiO_2 layer thickness was ~300 nm and the Si substrate was highly doped and served as the back gate. The prepared FEG device sample was then mounted on a chip carrier attached to the probe and installed inside the experimental system that allowed for in-situ electrical transport study. The setup allowed for the phosphorene FET to be placed in a controlled environment and exposed to different light sources (LEDs) while minimizing external light sources and keeping exposure to ambient conditions to a minimum. The system was also capable of heating the sample. It consisted of a sample probe inside a quartz reactor. The reactor had provisions for evacuation and exposure to various gasses at desired temperatures and pressures and it was placed inside a tube furnace for controlled heating. A chromel/alumel thermocouple was also mounted on the sample with silver epoxy to monitor the temperature. Transport characteristics were measured using Keithley picometer 6487 equipped with a voltage source and a Keithley 2400 source/measure unit. The LEDs used in these experiments were connected to separate contacts away from the substrate. However, they were positioned to ensure that the majority of light was directed towards the sample. As an added precaution, laboratory lights were cut off during measurements. The analysis chamber was evacuated to prevent sample degradation and shielded with light absorbing black-out material.

DFT Calculations

The overall computational calculations in this study was mainly carried out by employing the density functional theory (DFT) framework,[39, 40] as implemented in the Vienna Ab-initio Simulation Package (VASP).[41] The electron-ion interactions were described by the Projector Augmented Wave (PAW),[42] while electron exchange-correlation interactions were treated by the generalized gradient approximation (GGA)[43] in the scheme of Perdew Burke Ernzerhof (PBE).[44] The structural relaxation was performed using Congregate-Gradient algorithm[45] implemented in VASP. An energy cutoff was set to be 500 eV for the plane wave basis in all calculations, and the criteria for the convergences of energy and force in relaxation processes were set to be 10^{-5} eV and 10^{-4} eV/Å, respectively. For the benchmark, we calculated the structural and electronic properties of phosphorene (see Supporting Information). The optimized lattice constants for phosphorene are a = 3.306 Å, and b = 4.619 Å, which are consistent with the previous DFT results.[46-50] The band structure for the optimized phosphorene shows the directed bandgap behavior with the band gap of 0.82 eV is consistent with other DFT results[49, 51, 52] but underestimated compared with the experimental results (e.g., 1.45 eV reported in Ref.[53], or 2.05 eV reported in Ref.[54], or 2.09 eV reported in Ref.[37]). The underestimate in band gap in the LDA or GGA-PBE types of calculations will not affect the calculations on the adsorption of various gases on phosphorene, as pointed out in the calculations for the Na adsorption.[52]

A 3×3 supercell was chosen to study the adsorption of foreign gases on phosphorene monolayer. A vacuum space of 20 Å was set between adjacent layers to avoid any mirror interactions of gas molecules. The Brillouin zones (BZ) were sampled by 5×1×5 k-point meshes generated in accordance with the Monkhorst-Pack scheme in the calculations.[55] In the processes of investigating the response of phosphorene exposed under absorbers, one molecule was initially placed on the top of phosphorene with the ratio of molecule to phosphorene of 1:36. The combined system was fully relaxed. The adsorption energy per absorbed molecule on monolayer phosphorene (E_a) is defines as $E_a = E_{total} - E_{phosphorene} - E_{molecule}$, where E_{total}, $E_{phosphorene}$, and $E_{molecule}$ are the total energy of the combined system, the energy of the 3×3 pristine phosphorene (36 atoms), and the energy of the isolated molecule, respectively. The charge redistribution in real space is calculated by $\Delta\rho = \rho_{total} - \rho_{phosphorene} - \rho_{molecule}$, where ρ_{total}, $\rho_{phosphorene}$, and $\rho_{molecule}$ are the electron densities of the total, phosphorene, and molecule, respectively. The charge transfer is calculated using the Bader analysis.[56]

Conclusions

FETs structures were fabricated using phosphorene as the conducting channel and were evaluated for gas- and photo-

This journal is © The Royal Society of Chemistry 20xx
Please do not adjust margins

detection properties. Firstly, the FET performance was evaluated in various gas/chemical environments, including Ar, N_2O, H_2, and N_2H_4. Phosphorene's in-plane bonding leaves lone electron pairs of each phosphorus atom, which reacts with other atoms. By using a controlled environment, exposure of phosphorene to reducing or oxidizing gases caused major changes to its transport properties. It was found that hydrogen, which is a strong reducing agent, lowers the Schottky barrier by interacting with the phosphorene/Al interface. The relative resistance decreases as a result. It was also found the partial release of hydrogen can be done at room temperature. Hydrazine, which is also a reducing agent, had a similar effect; however, phosphorene more readily released the hydrazine molecules. This release may be impart caused by the increased size of the N_2H_4 molecule compared to H_2. On the other hand, nitrous oxide, which is an oxidizing agent, had the opposite effect. Relative resistance increased in phosphorene when exposed to N_2O. Due to the inert nature of argon, it had very little effect on phosphorene, which shows it to be suitable for safe storage of phosphorene-based devices. The FET structures were also evaluated as photodetectors by measuring in-situ photo-response during illumination with red and yellow LEDs. It was found that current modulation was lost in the FET every time that it was irradiated with light. Current modulation loss was observed for both, red and yellow, LEDs used. The above finding shows that care must be taken if phosphorene-based FETs are used in logic circuits, as visible light illumination can cause the transistor conducting channel to be open.

Conflicts of interest

The authors declare no conflict of interest.

Acknowledgements

This work was supported by the U.S. Department of Energy, Office of Science, Basic Energy Sciences, under Award # DE-SC0019348.

Notes and references

1. Y. Cai, G. Zhang and Y.-W. Zhang, *Scientific reports*, 2014, **4**, 6677.
2. S. Das and V. Jayaraman, *Progress in Materials Science*, 2014, **66**, 112-255.
3. A. Dey, *Materials Science and Engineering B-Advanced Functional Solid-State Materials*, 2018, **229**, 206-217.
4. Y.-F. Sun, S.-B. Liu, F.-L. Meng, J.-Y. Liu, Z. Jin, L.-T. Kong and J.-H. Liu, *Sensors*, 2012, **12**, 2610-2631.
5. T. Wagner, S. Haffer, C. Weinberger, D. Klaus and M. Tiemann, *Chemical Society Reviews*, 2013, **42**, 4036-4053.
6. D. J. Wales, J. Grand, V. P. Ting, R. D. Burke, K. J. Edler, C. R. Bowen, S. Mintova and A. D. Burrows, *Chemical Society Reviews*, 2015, **44**, 4290-4321.
7. S. S. Varghese, S. Lonkar, K. K. Singh, S. Swaminathan and A. Abdala, *Sensors and Actuators B-Chemical*, 2015, **218**, 160-183.
8. S. S. Varghese, S. H. Varghese, S. Swaminathan, K. K. Singh and V. Mittal, *Electronics*, 2015, **4**, 651-687.
9. S. Yang, C. Jiang and S.-H. Wei, *Applied Physics Reviews*, 2017, **4**, 021304.
10. W. Yang, L. Gan, H. Li and T. Zhai, *Inorganic Chemistry Frontiers*, 2016, **3**, 433-451.
11. M. Donarelli and L. Ottaviano, *Sensors (Basel)*, 2018, **18**, 3638.
12. S. Mao, J. Chang, H. Pu, G. Lu, Q. He, H. Zhang and J. Chen, *Chem Soc Rev*, 2017, **46**, 6872-6904.
13. X. Tang, A. Du and L. Kou, *Wiley Interdisciplinary Reviews: Computational Molecular Science*, 2018, **8**.
14. A. N. Abbas, B. Liu, L. Chen, Y. Ma, S. Cong, N. Aroonyadet, M. Koepf, T. Nilges and C. Zhou, *Acs Nano*, 2015, **9**, 5618-5624.
15. M. Akhtar, G. Anderson, R. Zhao, A. Alruqi, J. E. Mroczkowska, G. Sumanasekera and J. B. Jasinski, *Npj 2d Materials and Applications*, 2017, **1**, 5.
16. S. Cui, H. Pu, S. A. Wells, Z. Wen, S. Mao, J. Chang, M. C. Hersam and J. Chen, *Nature Communications*, 2015, **6**, 8632.
17. L. Kou, T. Frauenheim and C. Chen, *Journal of Physical Chemistry Letters*, 2014, **5**, 2675-2681.
18. M. Donarelli, L. Ottaviano, L. Giancaterini, G. Fioravanti, F. Perrozzi and C. Cantalini, *2d Materials*, 2016, **3**, 025002.
19. Z. Feng, B. Chen, S. Qian, L. Xu, L. Feng, Y. Yu, R. Zhang, J. Chen, Q. Li, Q. Li, C. Sun, H. Zhang, J. Liu, W. Pang and D. Zhang, *2d Materials*, 2016, **3**, 035021.
20. S. Shi, R. Hu, E. Wu, Q. Li, X. Chen, W. Guo, C. Sun, X. Hu, D. Zhang and J. Liu, *Nanotechnology*, 2018, **29**, 435502.
21. N. Suvansinpan, F. Hussain, G. Zhang, C. H. Chiu, Y. Cai and Y. W. Zhang, *Nanotechnology*, 2016, **27**, 065708.
22. A. A. Kistanov, Y. Q. Cai, K. Zhou, S. V. Dmitriev and Y. W. Zhang, *J Phys Chem C*, 2016, **120**, 6876-6884.
23. M. Buscema, D. J. Groenendijk, S. I. Blanter, G. A. Steele, H. S. J. van der Zant and A. Castellanos-Gomez, *Nano Letters*, 2014, **14**, 3347-3352.
24. J. Wu, G. K. W. Koon, D. Xiang, C. Han, C. T. Toh, E. S. Kulkarni, I. Verzhbitskiy, A. Carvalho, A. S. Rodin, S. P. Koenig, G. Eda, W. Chen, A. H. Castro Neto and B. Oezyilmaz, *Acs Nano*, 2015, **9**, 8070-8077.
25. Q. Guo, A. Pospischil, M. Bhuiyan, H. Jiang, H. Tian, D. Farmer, B. Deng, C. Li, S.-J. Han, H. Wang, Q. Xia, T.-P. Ma, T. Mueller and F. Xia, *Nano Letters*, 2016, **16**, 4648-4655.
26. J. Na, K. Park, J. T. Kim, W. K. Choi and Y.-W. Song, *Nanotechnology*, 2017, **28**, 085201.
27. S. C. Desai, A. H. Willitsford, G. U. Sumanasekera, M. Yu, W. Q. Tian, C. S. Jayanthi and S. Y. Wu, *Journal of Applied Physics*, 2010, **107**, 114509.
28. A. Alruqi, M. R. Khan Musa, R. Zhao, C. Zhang, J. B. Jasinski, M. Yu and G. Sumanasekera, *The Journal of Physical Chemistry C*, 2019.
29. B. Deb, S. Desai, G. U. Sumanasekera and M. K. Sunkara, *Nanotechnology*, 2007, **18**.
30. K. W. Adu, Q. Li, S. C. Desai, A. N. Sidorov, G. U. Sumanasekera and A. D. Lueking, *Langmuir*, 2009, **25**, 582-588.
31. A. N. Sidorov, D. K. Benjamin, Z. Jiang, A. Sherehiy, R. Jayasinghe, R. Stallard, G. U. Sumanasekera, Q. Yu, Z. Liu, W. Wu, H. Cao and Y. P. Chen, *Applied Physics Letters*, 2011, **99**.

This journal is © The Royal Society of Chemistry 20xx

Please do not adjust margins

32. S. Das, W. Zhang, M. Demarteau, A. Hoffmann, M. Dubey and A. Roelofs, *Nano letters*, 2014, **14**, 5733-5739.
33. S. Das, M. Demarteau and A. Roelofs, *ACS nano*, 2014, **8**, 11730-11738.
34. M. Garara, H. Benzidi, M. Lakhal, M. Louilidi, H. Ez-Zahraouy, A. El Kenz, M. Hamedoun, A. Benyoussef, A. Kara and O. Mounkachi, *International Journal of Hydrogen Energy*, 2019, **44**, 24829-24838.
35. Y. Cai, Q. Ke, G. Zhang and Y.-W. Zhang, *The Journal of Physical Chemistry C*, 2015, **119**, 3102-3110.
36. M. Koepf, N. Eckstein, D. Pfister, C. Grotz, I. Krueger, M. Greiwe, T. Hansen, H. Kohlmann and T. Nilges, *Journal of Crystal Growth*, 2014, **405**, 6-10.
37. M. Akhtar, C. Zhang, M. Rajapakse, M. R. K. Musa, M. Yu, G. Sumanasekera and J. B. Jasinski, *Physical Chemistry Chemical Physics*, 2019, **21**, 7298.
38. D. R. Mitchell, *Microscopy research and technique*, 2008, **71**, 588-593.
39. P. Hohenberg and W. Kohn, *Physical review*, 1964, **136**, B864.
40. W. Kohn and L. J. Sham, *Physical review*, 1965, **140**, A1133.
41. G. Kresse and J. Furthmüller, *Physical review B*, 1996, **54**, 11169.
42. P. E. Blöchl, *Physical Review B*, 1994, **50**, 17953.
43. J. P. Perdew, J. A. Chevary, S. H. Vosko, K. A. Jackson, M. R. Pederson, D. J. Singh and C. Fiolhais, *Physical Review B*, 1992, **46**, 6671.
44. J. P. Perdew, K. Burke and M. Ernzerhof, *Physical review letters*, 1996, **77**, 3865.
45. X. Gonze, *Physical Review B*, 1997, **55**, 10337.
46. R. Fei and L. Yang, *Applied Physics Letters*, 2014, **105**, 083120.
47. H. Liu, A. T. Neal, Z. Zhu, Z. Luo, X. Xu, D. Tománek and P. D. Ye, *ACS nano*, 2014, **8**, 4033-4041.
48. Q. Yao, C. Huang, Y. Yuan, Y. Liu, S. Liu, K. Deng and E. Kan, *The Journal of Physical Chemistry C*, 2015, **119**, 6923-6928.
49. S. Zhao, W. Kang and J. Xue, *Journal of Materials Chemistry A*, 2014, **2**, 19046-19052.
50. X. Liu, Y. Wen, Z. Chen, B. Shan and R. Chen, *Physical Chemistry Chemical Physics*, 2015, **17**, 16398-16404.
51. H. Liu, A. T. Neal, Z. Zhu, Z. Luo, X. F. Xu, D. Tomanek and P. D. D. Ye, *Acs Nano*, 2014, **8**, 4033-4041.
52. V. V. Kulish, O. I. Malyi, C. Persson and P. Wu, *Physical Chemistry Chemical Physics*, 2015, **17**, 13921-13928.
53. D. Er, J. Li, M. Naguib, Y. Gogotsi and V. B. Shenoy, *ACS applied materials & interfaces*, 2014, **6**, 11173-11179.
54. S. Grimme, *Journal of computational chemistry*, 2006, **27**, 1787-1799.
55. H. J. Monkhorst and J. D. Pack, *Physical review B*, 1976, **13**, 5188.
56. G. Henkelman, A. Arnaldsson and H. Jónsson, *Computational Materials Science*, 2006, **36**, 354-360.

 This journal is © The Royal Society of Chemistry 20xx

Please do not adjust margins

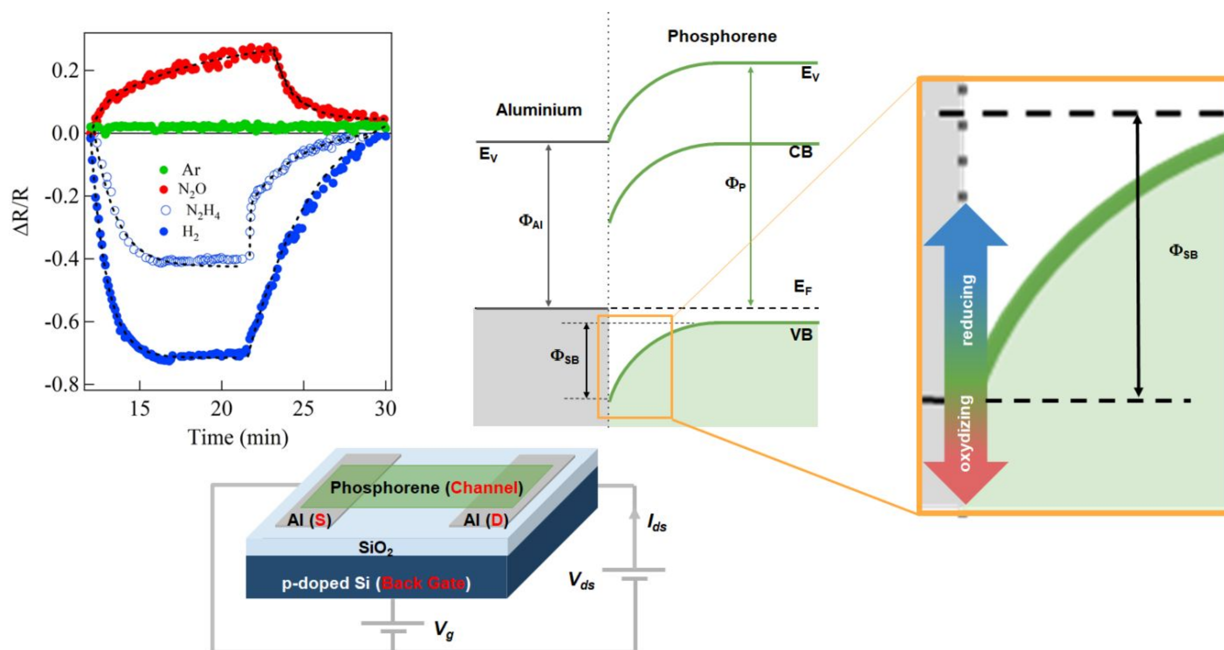

Phosphorene-based field effect transistors are fabricated and are shown to be highly sensitive gas and photodetectors. The sensing mechanism is explained using a Shottky barrier model at the phosphorene/metal contact interface.